Mon. Not. R. Astron. Soc. **000**, 1–13 (2005) Printed 8 January 2014 (MN LATEX style file v2.2)

The masses, radii and luminosities of the components of U Geminorum

T. Naylor[1] A. Allan[1] and K.S. Long[2]
[1] *School of Physics, University of Exeter, Stocker Road, Exeter EX4 4QL*
[2] *Space Telescope Science Institute, 3700 San Martin Drive, Baltimore, MD 21218, USA*

arXiv:astro-ph/0506351v1 15 Jun 2005

ABSTRACT
We present a phase-resolved spectroscopic study of the secondary star in the cataclysmic variable U Gem. We use our data to measure the radial velocity semi-amplitude, systemic velocity and rotational velocity of the secondary star. Combining this with literature data allows us to determine masses and radii for both the secondary star and white dwarf which are independent of any assumptions about their structure. We use these to compare their properties with those of field stars and find that both components follow field mass-radius relationships. The secondary star has the mass, radius, luminosity and photometric temperature of an M2 star, but a spectroscopic temperature of M4. The latter may well be due to a high metallicity. There is a troubling inconsistency between the radius of the white dwarf inferred from its gravitational redshift and inclination and that inferred from its temperature, flux, and astrometric distance.

We find that there are two fundamental limits to the accuracy of the parameters we can derive. First the radial velocity curve of the secondary star deviates from a sinusoid, in part because of its asphericity (which can be modelled) and in part because the line flux is not evenly distributed over its surface. Second we cannot be certain which spectral type is the best match for the lines of the secondary star, and the derived rotational velocity is a function of the spectral type of the template star used.

Key words: binaries: eclipsing – white dwarfs – stars: late-type – stars: fundamental parameters – stars: individual: U Gem – novae, cataclysmic variables.

1 INTRODUCTION

Precise radii and masses for the white dwarfs and late-type secondary stars in cataclysmic variables (CVs) are critical tests of our understanding of their evolution. For the secondary stars there has been a long debate as to whether they follow main-sequence mass-radius and mass-temperature relationships. These issues are reviewed in Smith & Dhillon (1998), who concluded that, although the CV data are consistent with the main sequence relationships, there is such a large scatter in the CV properties that the main-sequence relationships cannot be used to predict one quantity from another. Amongst the CVs with M-type secondaries, a large part of that scatter was driven by just two systems, IP Peg and U Gem. However, these are systems whose derived parameters should be amongst the most precise since they are eclipsing systems.

In an earlier paper we re-visited IP Peg (Beekman et al. 2000) and brought its parameters into line with those of the other CVs of similar orbital period, making U Gem a natural next target. However, there was another, pressing reason for re-visiting the parameters of this system, in that Long & Gilliland (1999) obtained a radial velocity curve for the white dwarf. This is the first radial velocity curve of a white dwarf obtained for any CV. This not only allows an almost assumption-free mass ratio $q(= M_2/M_1)$ to be derived, but also allows one to measure the gravitational redshift to the white dwarf, which given the white dwarf mass yields its radius. In principle, therefore, one could obtain independent measurements of both the mass and radius for each of the white dwarf and secondary star. There were three obstacles to such a complete analysis.

- There was no measurement of the rotational velocity of the secondary star ($v_2 \sin(i)$) from which its radius could be derived assuming only that it is phase locked.
- To measure the gravitational redshift of the white dwarf requires a measurement of the mean radial velocity of the red dwarf (γ_2). There were two measurements of this which conflicted.
- The radial velocity curve of the secondary star showed an apparent eccentricity. The best explanation for this would be that the line flux was not distributed evenly across the surface of the star, but without more data to examine the

residuals in detail, any corrections that should be applied to account for this were uncertain.

We therefore re-observed U Gem to solve these problems. In doing so we acquired a very high quality dataset, which illuminates various problems in parameter determination. This was part of a programme to obtain phase resolved red spectroscopy of cataclysmic variables and low-mass X-ray binaries with precise correction for the telluric absorption, so that one could study the TiO bands (Webb et al. 2002; Beekman et al. 2000; Webb et al. 2000). The observational techniques used in this paper should be seen as a further improvement on the ones described in those papers.

This paper is set out as follows. In Sections 2 and 3 we describe the data acquisition and reduction. The almost complete absence of interlocking assumptions then allows us to lay out the determination of the dynamical parameters in a very formal manner, discussing each parameter and its uncertainties in turn (Section 4). Our dataset is such that we discover that the uncertainties in both K_2 and $v_2\sin(i)$ are dominated by systematics. We then use these to obtain the physical parameters of interest in Section 5, before comparing them to field stars in our discussion (Section 6). We finally draw our conclusions in Section 7.

2 OBSERVATIONS

Spectra were obtained on the nights beginning January 4, 5, 6 and 7 2001 and January 17 2000 using the 2.5m Isaac Newton Telescope with the 235mm camera of the Intermediate Dispersion Spectrograph using a 1.5 arcsec slit. The slit width corresponds to approximately two pixels at the detector, and was a compromise. On the one hand narrowing it further would risk undersampling in wavelength space, which would compromise the precision with which we could measure velocities. Conversely, widening it would mean that velocity shifts would be introduced if the star moved across the width of the slit. The largest possible value of these shifts corresponds to the slit width, or $\pm$15km s^{-1}. Since the γ velocity of the white dwarf is only known to this precision, and in practice the seeing would ensure the shifts were smaller than this, the slit width was a reasonable compromise. In fact, as we shall discuss later, we found that these shifts could be measured and corrected, considerably improving the quality of our data.

The slit was orientated such that both U Gem and the $V \simeq 15$ star at α =07 55 07.08 δ =+21 59 19.7 (J2000) fell in the slit. For the majority of our spectra we used the R1200R grating which gave a resolution of 1.55Å and a coverage of 7480-8320Å at 0.83Å/pixel. This allowed us to cover the TiO band and KI lines at 7700Å and the NaI doublet at 8190Å. On the last night we used the R1800V grating to cover 7855-8335Å at 0.48Å/pixel with a resolution of 0.76Å, covering just the NaI doublet. We used an exposure of 420s for all our U Gem spectra. Since we required accurate radial velocities we took an arc spectrum after every two spectra of U Gem. We were also concerned to ensure that the signal-to-noise in our final mean spectra (which is around 350 for the lower resolution data) was not dominated by fringing on the CCD, so at the same time as we acquired an arc, we also obtained a tungsten lamp flatfield.

Since the primary aim of our observing procedure was to ensure excellent removal of the telluric absorption, we interspersed our observations of U Gem with observations of the rapidly rotating A0 star SAO78799 This star is relatively featureless in the range of interest, and so could be used to correct the telluric bands (see Section 3). After each observation of the A0 star we took an arc spectrum and a flatfield before moving the telescope.

We also required spectra of late-type stars for cross correlation and to determine an accurate spectral type for U Gem. These were obtained using the same instrumental setups as above. Again each observation was accompanied by a flatfield and arc, along with a spectrum of a nearby A0 star, which also had its own flatfield and arc.

3 SPECTRUM EXTRACTION

We treated all our observations of U Gem and the late-type stars in an identical fashion. Mean bias frames were subtracted from each image. We then created flatfields by calculating a correction with respect to a two dimensional polynomial fitted through each flatfield frame, and these were used to correct the arcs and star images. Spectra were then extracted from each stellar observation using an optimal technique (e.g. Horne 1986). For each such spectrum an arc was extracted from the appropriate exposure, from the same region of the detector as the star was extracted from. It was used to derive a polynomial relationship between pixel number and wavelength, which was used to wavelength calibrate the stellar spectra. Each target spectrum was then divided by the appropriate observation of an A0 star to remove the atmospheric absorption bands.

In an initial reduction of the data, we followed the telluric correction procedure developed in Beekman et al. (2000), where no interpolation of the telluric correction star onto the wavelength scale of the target was attempted as this can tend to smooth the spectra. Instead each target spectrum pixel is simply divided by the nearest pixel in wavelength from the A0 star spectrum.

In some cases this produced a rather poor telluric correction, and this was traced to different positions of the target star across the width of the slit, leading to small differences in the wavelength calibration. We therefore cross correlated all our target spectra and telluric correction spectra with one A-star spectrum, in the region 7624-7690Å which is dominated by telluric bandheads. We then applied the derived shifts to the wavelength values of each data point in all our target and telluric correction spectra. Before dividing we interpolated the telluric correction stars onto the same wavelength points as their respective targets using quadratic interpolation. We also normalised the correction spectrum such that it was one in the middle of its wavelength range to preserve the overall number of counts correctly for the target. This entire procedure improved some of the corrections dramatically. Equally importantly, though, it corrects for the drift of U Gem across the width of the slit, a point we shall return to in Section 4.1. We could not carry out this procedure for the higher resolution data, as there is not a region of such strong telluric absorption.

Each spectrum was corrected to the velocity of the solar system barycentre by allowing for the Earth's motion. Throughout the reduction process we propagated the un-

certainties from the optimal extraction. This allowed us to identify four spectra as of significantly lower signal-to-noise than the others (probably due to cloud), which were removed from the subsequent analysis. A further spectrum was removed due to a charged particle event in the region used for the velocity correction procedure. This left us with 118 low resolution and 59 high resolution spectra. Figure 1 shows our final summed spectra, shifted into the reference frame of the secondary star.

The 118 lower resolution spectra, and corresponding mean late-type star spectra are available via the CDS, or from http://www.astro.ex.ac.uk/people/timn/UGem/description.html.

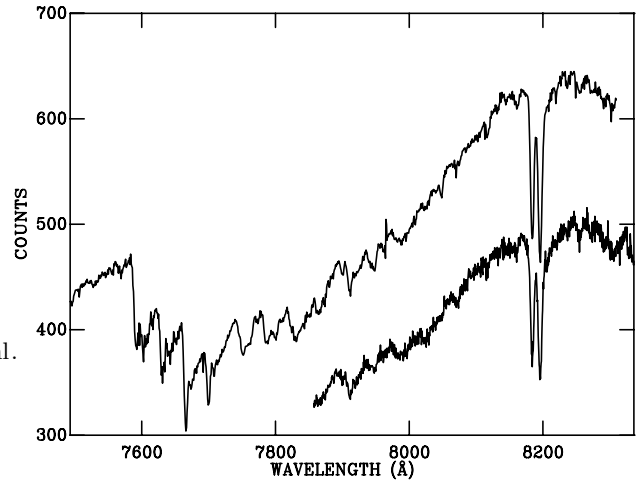

Figure 1. The mean of all spectra, summed into the rest frame of the secondary star using the parameters derived from the NaI lines using GJ213 as the spectral type template. The upper spectrum is the sum of the lower resolution data, the lower spectrum the higher resolution data. The higher resolution data have been multiplied by 1.8 (the difference in pixel size in wavelength space).

4 EXTRACTING THE DYNAMICAL PARAMETERS

There are three parameters that we were interested in extracting from our spectra. The observed radial velocity semi-amplitude of the secondary star, before correction for inclination (K_2); the rotational velocity of the secondary star, again before allowing for inclination ($v_2\sin(i)$); and the mean velocity of the secondary star (γ_2). In principle we have to measure all three parameters simultaneously. For example, we need a broadened spectral type template to cross-correlate against our individual U Gem spectra to obtain K_2, but can only obtain that by first velocity shifting all the individual spectra into the rest frame of the secondary star and summing them. Of course we cannot do this without first knowing K_2. We therefore adopted an iterative procedure outlined in the next two paragraphs, with each stage described in detail in the subsections below.

We began by analysing the lower resolution spectra. An inital radial velocity curve was extracted by cross correlating the NaI region of the U Gem spectra against a spectral type template. A fit to this gave an initial radial velocity semi-amplitude which we used to remove the orbital motion of the secondary star by shifting each spectrum in velocity. However, it was clear that the radial velocity curve was significantly non-sinusoidal between phases 0.25 and 0.75 (see Section 4.1.2 and Figures 3 and 4), and so we restricted these sums to the data outside this phase range. We then measured the velocity shift between the summed spectrum and the spectral type template, and then shifted the standard, and broadened it so its apparent rotational velocity matched that of the secondary star. We next re-cross correlated each U Gem spectrum with the broadened template to create a new radial velocity curve, from which we could again extract radial velocity curve parameters. We iterated around this procedure until the change in the velocity shift we applied to the spectral type template converged to within one km s^{-1}. Having obtained an initial radial velocity solution from the NaI region using one spectral type template we then used this as the starting parameters for using each spectral type template for both the NaI and KI/TiO regions.

As there are a smaller number of high resolution spectra, and they could not be corrected in velocity for the slit drift (see Section 3) we have used them only to measure $v_2\sin(i)$. Thus we coadded them using the K_2 found from the lower resolution data, and then fitted broadened templates, again using spectra from only phases 0.75 to 0.25.

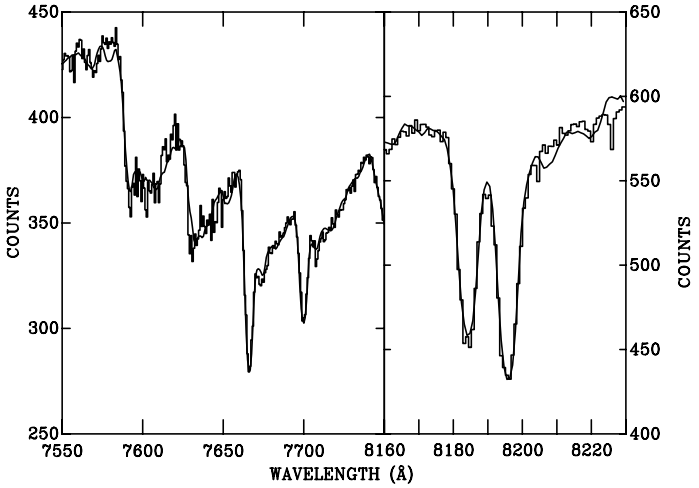

Figure 2. The mean of the low resolution spectra between phases 0.75 and 0.25 (histogram) with the best fit velocity broadened spectrum of GJ213 (line) overlaid. The wavelength regions are those over which the fitting was performed.

Aside from the dynamical parameters, the final output from this procedure is a spectrum in the rest frame of the secondary star. We show these spectra for both the high and low resolution data in Figure 1. In addition, Figure 2 shows the comparison between a broadened template star, and the sum of the spectra between phase 0.75 and 0.25 for the regions we used for the cross-correlation and $v_2\sin(i)$ fitting.

Table 1. Measured radial velocities from the NaI feature in the lower resolution spectra. The columns give the barycentric Julian Date for the middle of the exposure, the calculated phase for the exposure, the image number, radial velocity and uncertainty. The uncertainties are scaled to give a χ^2_ν of one for a circular fit. All exposures are of 420s duration.

BJD	Phase	Image Number	RV (km s^{-1})	Uncertainty (km s^{-1})
2 451 561.43994	0.5544	206090	-122	34
2 451 561.45081	0.6158	206094	-219	32
2 451 561.45612	0.6458	206095	-247	29
2 451 914.41589	0.8262	243111	-253	11
2 451 914.42090	0.8545	243112	-224	10
2 451 914.42700	0.8890	243115	-185	11
2 451 914.43201	0.9173	243116	-141	11
2 451 914.44177	0.9725	243123	-49	10
2 451 914.44672	0.0005	243124	4	11
2 451 914.45264	0.0339	243127	63	10
2 451 914.45758	0.0619	243128	121	9
2 451 914.46594	0.1091	243135	193	9
2 451 914.47095	0.1374	243136	239	9
2 451 914.47687	0.1709	243139	262	9
2 451 914.48181	0.1988	243140	279	8
2 451 914.49042	0.2475	243146	299	9
2 451 914.49542	0.2758	243147	293	9
2 451 914.50122	0.3085	243150	280	8
2 451 914.50616	0.3365	243151	268	8
2 451 914.51453	0.3838	243157	210	11
2 451 914.51947	0.4117	243158	160	10
2 451 914.52527	0.4445	243161	106	10
2 451 914.53027	0.4728	243162	53	12
2 451 914.53937	0.5242	243168	-65	9
2 451 914.54437	0.5525	243169	-125	8
2 451 914.55017	0.5853	243172	-175	9
2 451 914.55518	0.6135	243173	-218	8
2 451 914.56470	0.6674	243180	-266	10
2 451 914.56964	0.6953	243181	-293	8
2 451 914.57550	0.7284	243184	-302	8
2 451 914.58044	0.7564	243185	-282	8
2 451 914.58881	0.8036	243191	-283	8
2 451 914.59375	0.8316	243192	-251	8
2 451 914.59961	0.8647	243195	-217	8
2 451 914.60455	0.8927	243196	-188	8
2 451 914.61292	0.9399	243202	-118	8
2 451 914.61786	0.9679	243203	-73	8
2 451 914.62372	0.0010	243206	3	9
2 451 914.62866	0.0289	243207	60	12
2 451 914.63660	0.0738	243213	131	11
2 451 914.64160	0.1021	243214	181	11
2 451 914.64758	0.1359	243217	224	13
2 451 914.65253	0.1638	243218	254	10
2 451 914.65753	0.1921	243219	274	9
2 451 914.66583	0.2391	243225	282	9
2 451 914.67084	0.2673	243226	285	11
2 451 914.67657	0.2998	243229	287	9
2 451 914.68158	0.3281	243230	269	8
2 451 914.68988	0.3750	243236	224	8
2 451 914.69482	0.4029	243237	182	8
2 451 914.70062	0.4357	243240	128	8
2 451 914.70557	0.4637	243241	83	8
2 451 914.77521	0.8573	243272	-227	10
2 451 914.78015	0.8853	243273	-192	11
2 451 914.79144	0.9491	243280	-91	12
2 451 914.79639	0.9770	243281	-36	12
2 451 915.44385	0.6369	243399	-233	9
2 451 915.44879	0.6649	243400	-255	9
2 451 915.45428	0.6959	243403	-292	9
2 451 915.45923	0.7239	243404	-292	8
2 451 915.46637	0.7643	243408	-289	8
2 451 915.47131	0.7922	243409	-287	8
2 451 915.47687	0.8236	243412	-262	8
2 451 915.48181	0.8515	243413	-235	8
2 451 915.48926	0.8936	243417	-184	8
2 451 915.49420	0.9216	243418	-137	8
2 451 915.49976	0.9530	243421	-97	9
2 451 915.50470	0.9809	243422	-33	11
2 451 915.51202	0.0223	243426	43	18
2 451 915.51697	0.0503	243427	63	39
2 451 915.52252	0.0817	243430	147	19
2 451 915.52747	0.1096	243431	208	20
2 451 915.53467	0.1503	243435	251	21
2 451 915.53961	0.1783	243436	284	23
2 451 915.55011	0.2376	243440	311	17
2 451 915.56897	0.3442	243445	253	14
2 451 915.57391	0.3722	243446	226	12
2 451 915.57941	0.4032	243449	192	13
2 451 915.58429	0.4308	243450	135	12
2 451 916.43011	0.2120	243541	287	9
2 451 916.43506	0.2400	243542	293	9
2 451 916.44061	0.2714	243545	290	9
2 451 916.44550	0.2990	243546	291	9
2 451 916.45367	0.3452	243550	248	9
2 451 916.45862	0.3732	243551	220	9
2 451 916.46417	0.4046	243554	201	24
2 451 916.50348	0.6267	243559	-231	9
2 451 916.50842	0.6547	243560	-256	8
2 451 916.51398	0.6861	243563	-279	8
2 451 916.51892	0.7140	243564	-297	8
2 451 916.52625	0.7554	243568	-291	11
2 451 916.53119	0.7834	243569	-286	9
2 451 916.53674	0.8148	243572	-271	8
2 451 916.54169	0.8427	243573	-247	8
2 451 916.54938	0.8862	243577	-200	9
2 451 916.55432	0.9141	243578	-159	9
2 451 916.55981	0.9452	243581	-101	10
2 451 916.56482	0.9735	243582	-55	9
2 451 916.57239	0.0163	243586	20	10
2 451 916.57733	0.0442	243587	63	9
2 451 916.58282	0.0753	243590	141	8
2 451 916.58777	0.1032	243591	174	8
2 451 916.59698	0.1553	243595	242	8
2 451 916.60193	0.1832	243596	277	8
2 451 916.60748	0.2146	243599	289	8
2 451 916.61243	0.2426	243600	286	8
2 451 916.63782	0.3861	243632	209	8
2 451 916.64276	0.4141	243633	162	9
2 451 916.64838	0.4458	243636	105	9
2 451 916.65338	0.4741	243637	53	9
2 451 916.66052	0.5145	243641	-28	10
2 451 916.66553	0.5428	243642	-96	14
2 451 916.67114	0.5745	243645	-152	12
2 451 916.67615	0.6028	243646	-193	16
2 451 916.68915	0.6763	243651	-267	11
2 451 916.69476	0.7080	243654	-275	11
2 451 916.69977	0.7363	243655	-306	20
2 451 916.70721	0.7784	243659	-269	25

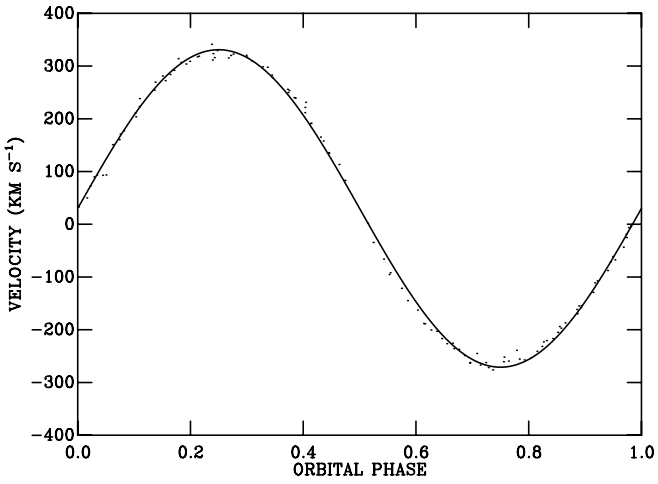

Figure 3. The radial velocity curve extracted from the low resolution data by cross-correlation of the NaI lines with the M4.0 star GJ213, corrected to the solar system barycentre. The curve is the best (circular) fit to the data.

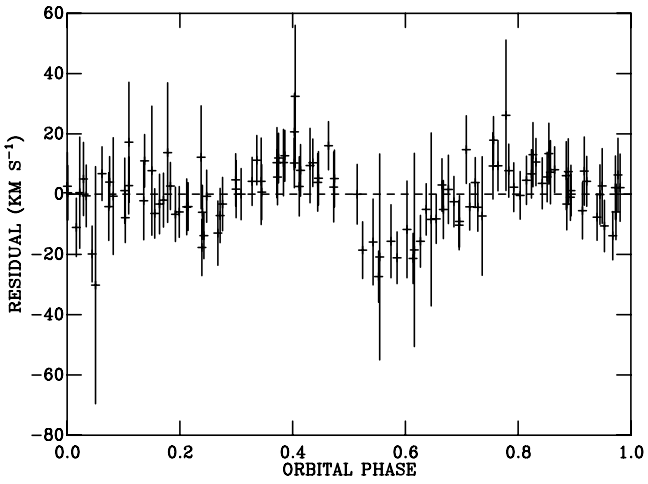

Figure 4. The residuals about the fit shown in Figure 3. The error bars are the relative uncertainties scaled to give a χ^2_ν of one.

4.1 K_2

4.1.1 The radial velocity curve

We cross-correlated the KI/TiO (7550-7750Å) and NaI (8160-8230Å) regions of each spectrum with that of each spectral type template. We chose the upper limit of the TiO region to avoid the feature at 7773Å, which is probably OI (Friend et al. 1988). We then fitted a sine curve to the resulting radial velocity curves, with the period fixed at that of Marsh et al. (1990). Each velocity was weighted according to the calculated signal-to-noise in the spectrum from which it was derived, using the region 7800-8000Å for the low resolution data and 8140-8250Å for the high resolution data. Since we only have relative weights for the data points, we cannot assign absolute values of χ^2, but the relative change in χ^2 between the different fits is meaningful. We found that all the NaI fits have χ^2 values within ± 2 percent of each other, but the KI/TiO region gives values 20 to 80 percent larger. We therefore decided that NaI provides a better solution, and in Figure 3 we show the radial velocity curve and the best fit and in Figure 4 the residuals about that fit. Table 1 gives the individual radial velocity points.

We note in passing that the RMS of the fits fell considerably between the initial and final radial velocity curves. This is presumably because the broadened templates match the data better, and so yield better cross-correlation functions. This leads us to believe that the reason we obtained better results in Beekman et al. (2000) from cross-correlating with a summed spectrum of IP Peg rather than the template stars was that the latter were not broadened.

4.1.2 The nature of the deviations

It is immediately obvious from Figures 3 and 4 that there are systematic deviations from the best fit. There are two obvious hypotheses which might explain these deviations. The first is a region of reduced NaI absorption flux around the inner Lagrangian point. There is observational backing for such an hypothesis, since surface mapping of the secondary star using the radial velocity data available prior to the current work, maps the observed apparent eccentricity into a region of reduced NaI absorption (Davey & Smith 1992). Such a region would lead to a lack of NaI absorption on the hemisphere of the secondary star rotating towards the observer at phases around 0.4, and away from the observer at 0.6. Since removing flux from the blueward wing of the line will result in an apparent redshift, this would, apparently, explain the residuals. There are a range of possible physical causes for such a region, but it is unclear whether the region needs to be hotter or cooler than the immaculate photosphere to cause a deficit in NaI absorption. Heating will cause the overall continuum flux to rise, but will also decrease the equivalent width of the NaI line. Which effect will dominate the change in flux is unclear, though the irradiation calculations of Brett & Smith (1993) do yield the required decrease in NaI flux. Cool spots on the other hand may be caused by by magnetic activity (see the observations of Webb et al. 2002, and references therein), or by a combination of limb and gravity darkening. Again the sign of the effect on the NaI flux is unclear as in the former case there is is also a gravity effect, and in the latter the line limb and gravity darkening co-efficients are essentially unknown. Nevertheless, it appears that a spot resulting in a decrease in the NaI (and KI) flux at the stellar surface could explain the observations.

The second obvious candidate is absorption of light from the secondary star as it passes through the accretion disc. Littlefair et al. (2001) have demonstrated the importance of such "mirror eclipses" in the IR, and finding their counterpart in optical data would clearly be of importance. A mirror eclipse would create further absorption in the spectrum. At phase 0.4, the star would be moving behind material moving away from the observer, and at phase 0.6 material moving towards them. This excess absorption would again create the observed effect.

There is a very obvious way to choose between these models, by comparing the spectra at phases 0.4 and 0.6 with our summed spectrum taken from phases 0.75 to 0.25. The

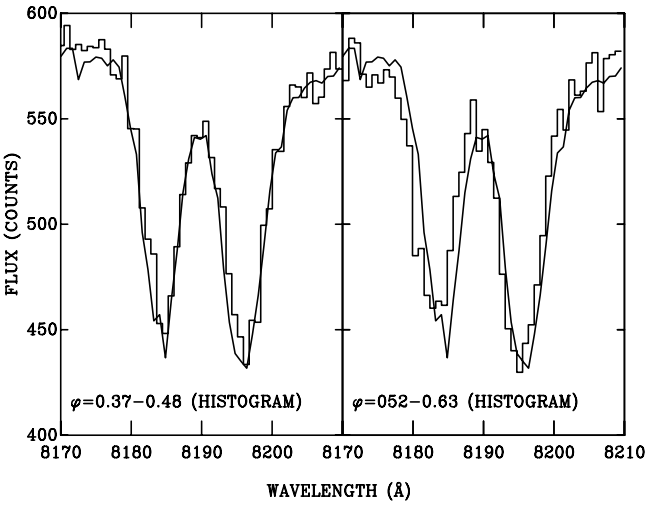

Figure 5. The mean of the spectra between phase 0.75 and 0.25 (solid line) compared with the mean of spectra in the phase range 0.37 to 0.48 (left) and 0.52 to 0.63 (right).

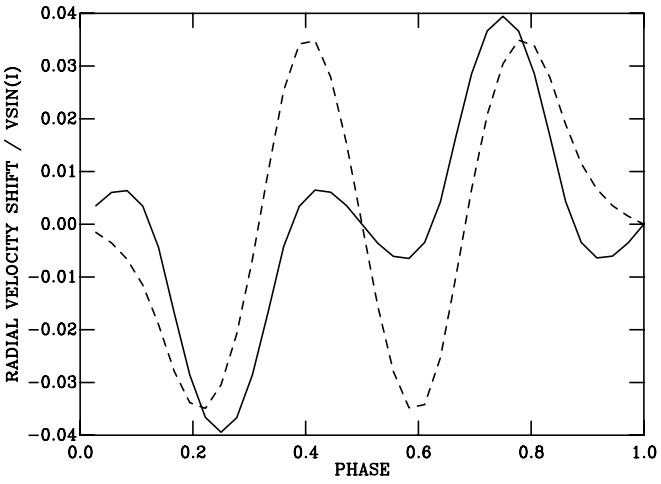

Figure 6. The radial velocity shifts expected from two different models of the secondary star. The solid line is for a uniform distribution of line flux over a Roche-lobe filling secondary star for a q of 1/3. The dashed line shows the result of adding gravity darkening.

dark spot model predicts, at phase 0.4, that there will be a lack of flux on the blue wings of the line, whilst a mirror eclipse would predict extra absorption on the red wing. Figure 5 shows these spectra, scaled so that the continuum values are similar to the phase 0.75 to 0.25 sum, which has been overlaid on the same plots. It is reassuring that with such a simple scaling the depths of the NaI lines match so well; it implies that the majority of the variability and of the flux originates from the secondary star. If this was not the case the equivalent width of the NaI lines would not be so constant.

The case at phase 0.4 seems clear-cut. The red wings of the lines are co-incident, but the blue wing of the phase 0.4 spectrum is consistently redder by between a half and one pixel (15-30 km s^{-1}). This lack of blue absorption at this phase supports the idea of a spot. At phase 0.6 the situation is more ambiguous, with the whole line being shifted bluewards by between a half and one and a half pixels (15-45 km s^{-1}).

To assess the credibility of the spot model further, we modelled the radial velocity curve of a Roche-lobe filling star using a modified version of the code first presented in Shahbaz et al. (1993). We assigned a radial velocity to each point on the grid which covers the surface of the secondary star and used the fluxes from each point to produce a line profile at that phase. As is usual in modelling rotational profiles, we normalised the velocity scale for the profile in terms of $v_2\sin(i)$. Throughout the modelling we used a mass ratio $q = M_2/M_1$ =1/3, and inclination of 67 degrees. We calculated the radial velocity deviations the model would produce from a circular orbit as the first moment of the profile. As a baseline, we first calculated a model with no limb or gravity darkening. Such a model is equivalent to assuming that the NaI flux is uniform across the surface of the star, and does not depend on the angle an element is viewed at. Figure 6 shows the result, with deviations of the correct order ($0.04v_2\sin(i)$ $\simeq$12km s^{-1}), but at the wrong phases (0.25 and 0.75). These deviations are due to the asphericity of the secondary star. The inner Lagrangian point moves faster than the mean surface of the secondary, and so when on the limb of the secondary moving towards the observer (as at phase 0.25) it produces a small blue shift with respect to the expected radial velocity curve. This effect can be observed in our residuals in Figure 4 but is not the dominating "problem".

We next placed a spot on the inner Lagrangian point. Whilst we could have achieved this by an arbitrary dimming of the flux, we chose instead to include gravity darkening in our model, by using a "standard" gravity darkening coefficient for a convective envelope of 0.08 (Lucy 1967). We did this not with the idea of establishing that gravity darkening is the cause of the dark spot, but simply to establish whether it has the correct order-of-magnitude. The result of this is again shown in Figure 6, where it can be seen that it results in two more peaks in the radial velocity curve residual, of roughly the same size as those due to the asphericity of the secondary star, but now at phase 0.4 and 0.6.

Before comparing this model with our residuals we subtracted from it the best fitting sinusoid with a fixed phase zero to simulate the effect of our fitting process. This has an amplitude of $0.01v_2\sin(i)$. The result is shown in Figure 7, where we have assumed a $v_2\sin(i)$ of 115 km s^{-1} (see Section 4.3). The deviations due to the asphericity of the secondary star are well modelled, but it is clear we need a somewhat darker spot to reproduce the data. Furthermore, the dark spot deviations are obviously asymmetric, which cannot be explained by this simple model. However, further modelling lies beyond the scope of this work, our aim is simply to establish how far these deviations from a perfect sinusoid affect our derived parameters.

4.1.3 Deciding a value and an uncertainty

The important result from Section 4.1.2 is that the result of fitting a sinusoid to the radial velocity deviations due to both the asphericity of the secondary star, and the inner

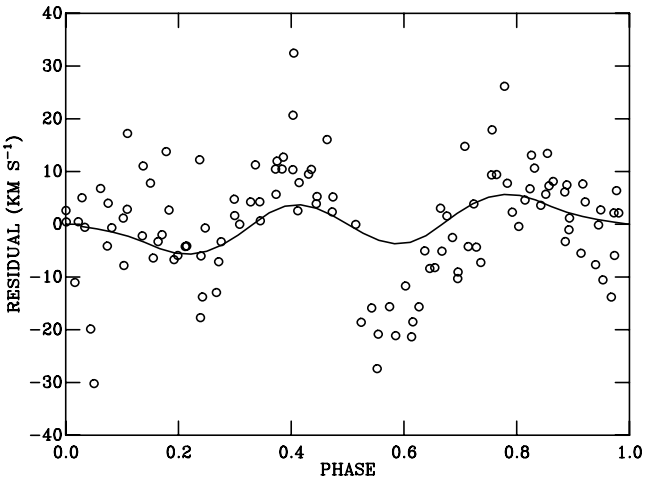

Figure 7. The solid line is the model for the residuals which includes both the Roche geometry and gravity darkening (the dashed line of Figure 6). We have subtracted from this model the best fitting sine wave with the phase fixed, and then scaled it using a $v_2\sin(i)$ of 115 km s^{-1}. The circles are the residuals presented in Figure 5.

Lagrangian dark spot is about $0.01v_2\sin(i)$, or about 1.2 km s^{-1}. Clearly this is not the entire story, it looks as though the dark spot is darker than our predictions, and the asymmetry remains unexplained. We therefore apply our predicted correction, since the effects modelled in it should be present, but we should also be aware that there are probably further corrections of a similar order. If we simply take a mean of the NaI values in Table 2 and make this correction our final answer is 300 km s^{-1}. Deciding an uncertainty for this value is not trivial. We can derive a statistical uncertainty for a the sine fit by scaling the relative error bars to yield a χ^2_ν of 1, which yields around 1 km s^{-1}. Of course, if we included the effects of asphericity and the dark spot in our model the size of error bar required to reach a χ^2_ν of one would decline, along with our final uncertainty estimate. Conversely, it is clear that our symmetric model will never fit both the deviations at phase 0.4 and 0.6 to better than 5km s^{-1}. Even if we used that as an uncertainty, it would never dominate the uncertainties in our final parameters for U Gem. Therefore we will ignore the uncertainty in K_2 throughout this paper, and leave any future users of this measurement to use the above discussion to choose an appropriate uncertainty for their use.

4.1.4 Comparison with previous values

We can now, finally, understand the apparent eccentricities found by Friend et al. (1990) and Wade (1981) of 0.027 and 0.086 respectively. If we fit our own data with an elliptical orbit we also obtain an eccentricity of about 0.024, with a significant decrease in the residuals caused by the inner Lagrangian dark spot. So, it seems clear that the measured eccentricities in the orbit of U Gem are caused by these effects, but that the correction for this, derived in the previous section seems to be small, $\sim$1 km s^{-1}. Therefore, to compare our value for the radial velocity semi-amplitude of the secondary star with previous work, it seems best to use the raw K_2, i.e. without the corrections suggested either by ourselves or Friend et al. (1990). Our value of 302km s^{-1} should therefore be compared with 309 ± 3km s^{-1} (Friend et al. 1990) and 283 ± 15 (Wade 1981). Given the uncertainty we have about our errors, these values are in agreement.

4.2 Spectroscopic Phase Zero

Although this is not important for our work here, we can also use our radial velocity curve to derive a measurement of spectroscopic phase zero. We obtain a time of TDB 2 451 915.8618 or HJD 2 451 915.8611. The uncertainty is about 0.0002 day. This lies about 0.0006 day or about 1.5σ away from the extrapolation of the Marsh et al. (1990) ephemeris, after taking into account the uncertainties in the ephemeris itself.

4.3 $V_2\sin(i)$

4.3.1 Method

Examination of Figure 4 shows that there are significant deviations from the radial velocity curve between phases 0.25 and 0.75, as one might expect as a result of an inner Lagrangian dark spot. This implies that the dark spot significantly distorts the line profile, and so if we are to determine the rotational velocity of the secondary star it is sensible to omit these phases. Therefore we co-added the spectra between phases 0.75 and 0.25 using the derived semi-amplitude, and then fitted them in the same wavelength regions used to derive K_2, to a broadened version of the spectral type templates, along with a smoothly varying continuum. We broadened the spectral type template using the analytical function appropriate for a spherical star.

Each of our spectra is a time average, during which the secondary star will move along its orbit, adding a further broadening to the line profiles. To check that we had succeeded in making our observations short enough to ensure this effect was negligible we calculated the maximum extra broadening any spectrum should have (30 km s^{-1}). We then pre-broadened the spectrum of the spectral-type standard by this amount, and repeated our fitting procedure. This changed the derived $v_2\sin(i)$ by < 4 km s^{-1}, and so the effects of velocity smearing can be neglected.

As discussed in Section 4.1.2, the non-sphericity of the secondary star has a significant effect on the radial velocity curve. Shahbaz (1998) shows that we might also expect it to affect the line profile broadening, making it significantly different from the spherical star broadening assumed in our model. To test this we used our Roche model to create a series of line profiles from phase 0.25 to 0.75, and averaged them. We then fitted this profile with our spherical model, and found that the difference in derived $v_2\sin(i)$ was less than 2 percent. This is far smaller than other uncertainties in our analysis and so can be safely ignored.

4.3.2 Deciding a value and an uncertainty

The statistical uncertainties in our values can be estimated by creating a χ^2 grid for the two parameters, which are the

fraction of the light from the secondary star and the rotational broadening. At each point in the grid we calculated the value of χ^2, and then re-normalised the grid so that the best fitting model gave a χ^2_ν of one. Our 1σ uncertainty is then simply the range of values of $v_2\sin(i)$ which lie within a χ^2 (not χ^2_ν) of 2.3 of the best fit. This procedure is conservative in the sense that the calculated uncertainty would be smaller if we did not rescale χ^2. This gives uncertainties around 10 km s^{-1} for either of the two regions used at low resolution, or the high resolution data.

In addition to the statistical uncertainty, we must also consider the fact that there is a very obvious correlation between the values of $v_2\sin(i)$ given in Table 2 and the spectral type of the template used for the cross-correlation. Later spectral types gave smaller values of $v_2\sin(i)$, presumably because the lines in these stars are closer to saturation, and so need less broadening to match the width of the lines of U Gem. As we shall discuss in Section 6.1 we cannot use the spectral type of the secondary star as a guide, and so we are forced to look at the values of χ^2_ν to decide which fits are the most appropriate. The best NaI fits cover the range 120-130km s^{-1}, whilst KI/TiO cover 105-130 km s^{-1}. We therefore adopt a value of 115$\pm$15km s^{-1} for $v_2\sin(i)$, where the uncertainty is driven by not knowing the correct template to use, as this is larger than the uncertainty derived from the χ^2 analysis.

4.4 γ_2

4.4.1 Method

To obtain γ_2 we calculated the difference in velocity between each spectral type template and the mean, velocity shifted U Gem spectrum it produced, and then added the barycentric radial velocity of the template obtained from the literature. The obvious course is to take a simple mean of all the derived γ velocities, but before doing so we will examine the values obtained as a function of both lines measured, and spectral type standard used.

The most obviously discrepant values are those given by GJ1111. As indicated by the values of χ^2_ν in Table 2, the broadened template for this star is a very bad fit to the data. The next most discrepant values are those for GL490B. Here the discrepancy is almost certainly due to the γ velocity assumed for GL490B. Most of the template star velocities are from Gizis et al. (2002), and have a accuracy of better than 1.5 km s^{-1}, but two objects (GJ463 and GL490B) are from Reid et al. (1995). Although Reid et al. (1995) estimate the accuracy of their velocity measurements at 10km s^{-1}, we calculated the differences between a given star's measured velocity in Reid et al. (1995) and that in Marcy et al. (1987). The velocities in the latter have uncertainties of less than 1km s^{-1}. This gave an RMS of 14km s^{-1} for the 58 stars. Using this uncertainty, the measurements for GL490B are in agreement with the other measurements, excepting GJ1111.

To check that different spectral features did not give discrepant values for γ_2 we could have taken a simple mean of the velocities for the five remaining objects (four in the case of the higher resolution data) for each wavelength range. However, if we are to exclude GL490B on the grounds it has a poor determination of its systemic velocity, we must also exclude GJ463. After removing this star we see from the RMS (which is, admittedly derived from a small number of values) that the KI/TiO measurements are in agreement with both the high and low resolution NaI velocities.

4.4.2 Deciding a value and an uncertainty

Given the above discussion, it seems we can take a very direct approach and simply take the mean of all the measurements for the four good radial velocity standards. This gives a final measurement of 29$\pm$6 km s^{-1}, where the uncertainty is simply the standard error. In principle the errors in the measurements of the velocities of the standards will add correlations to our 11 measurements, but this is small compared with our final uncertainty. We may also have added a little noise by including the high resolution data (which originate from fewer spectra), but as we shall see later, the final uncertainty in the gravitational redshift of the white dwarf is governed not by this error, but by the uncertainty in γ_1.

4.4.3 Comparison with previous work

One of the most important aims of this work was to decide between the two contradictory measurements for γ_2 of 46$\pm$6 km s^{-1} Friend et al. (1990) and 84.9 $\pm$ 9.9 Wade (1981). Our data clearly favour the Friend et al. (1990) result, the difference between the two being at the 2σ level.

4.5 Final dynamical parameters

We summarise our values for the dynamical parameters as follows. K_2=300 km s^{-1}, with an uncertainty which is unclear, but small enough to have an insignificant impact on what follows. $v_2\sin(i)$=115$\pm$15km s^{-1}, where the uncertainty in the appropriate spectral type to use dominates our error budget. γ_2=29$\pm$6 km s^{-1}, where the signal-to-noise in our spectra is probably responsible for the majority of the uncertainty.

5 PHYSICAL PARAMETERS

We can now use our measurements of the dynamical parameters, to derive the physical parameters of interest.

5.1 The Mass Ratio

The mass ratio M_2/M_1 is simply the ratio K_1/K_2. Long & Gilliland (1999) give $K_1 = 107.1\pm2.1$ km s^{-1}, which when combined with our value of K_2 yields 0.357$\pm$0.007.

5.2 The Inclination

The eclipse morphology of U Gem gives quite tight constraints on the inclination. The eclipse is thought to be that of the bright spot and edge of the disc, not the white dwarf (Warner & Nather 1971), an idea supported by the delay between spectroscopic phase zero and mid-eclipse (Wade 1981). For a q of 0.357, the system would eclipse the white dwarf if $i >$74 degrees. For our derived mass ratio we expect the disc to be no larger than $0.66R_{L1}$ (Paczynski 1977), a

Table 2. Measured Parameters. Columns 1-3 give the spectral type, name and assumed γ velocity for each spectral type standard. Columns 4-5 give the values of K_2 derived from the NaI and KI/TiO features in the lower resolution spectra. Columns 6-11 give the results for velocity broadening the spectral type templates to match the mean U Gem spectrum. For each parameter we give the values derived from the NaI and KI/TiO features in the lower resolution spectra, and from the NaI feature in the higher resolution spectra. Thus columns 6-8 give the best fitting values of $v_2\sin(i)$ and (in brackets) the associated χ^2_ν, and columns 9-11 the implied fraction of the light originating from the secondary star. Columns 12-14 give the derived values of γ_2 for U Gem, again from the lower resolution NaI and KI/TiO range, and the higher resolution NaI range.

Radial Velocity standard			K_2 (km s^{-1})		$v_2\sin(i)$ (km s^{-1})			% from secondary			γ_2 (km s^{-1})		
Type	Name	γ (km s^{-1})	NaI	KI/TiO	NaI	KI/TiO	Hi	NaI	KI/TiO	Hi	NaI	KI/TiO	Hi
(1)	(2)	(3)	(4)	(5)	(6)	(7)	(8)	(9)	(10)	(11)	(12)	(13)	(14)
M3	GJ463	21	302	305	142 (3.1)	143 (2.8)		116	109		38	43	
M3	GL109	30	301	303	139 (2.9)	140 (2.4)		104	84		30	34	
M4	GL490B	-23	301	303	130 (2.3)	116 (2.3)		76	51		11	18	
M4	GJ213	106	301	303	132 (2.7)	129 (2.3)	121 (1.0)	98	64	77	18	30	30
M5	GL51	-7	302	300	119 (2.6)	105 (2.2)	118 (1.1)	58	38	67	24	37	25
M5.5	GL65A	22	301	296	118 (2.9)	96 (2.7)	106 (1.1)	61	31	53	25	39	28
M6	GJ1111	8	301	289	110 (3.1)	128 (3.4)	110 (1.1)	50	26	44	43	66	48
Mean (GL109, GJ213, GL51, GL65A)											24	34	27
Standard error											5	4	3

radius which would just be eclipsed if i=62 degrees. The inclination must, therefore, lie in the range 68±6 degrees. Conveniently, the mid-point of this range is close to the 69±2 degrees given by the most recent of determinations of the inclination from detailed bright spot analysis (Smak 2001, and references therein).

5.3 The mass of the secondary star

From Kepler's Law it is easy to show that the mass of the secondary star is

$$M_2 = \frac{K_1^3 P}{2\pi G \sin^3(i)} \left(1 + \frac{K_2}{K_1}\right)^2. \quad (1)$$

Given our values derived above, this gives

$$M_2 = \frac{0.34 \pm 0.02 M_\odot}{\sin^3(i)}, \quad (2)$$

where the uncertainty originates from the uncertainty in K_1. If we wish to derive a value independent of $\sin(i)$, then taking the range of values of the inclination from above, we find that $M_2 = 0.44 \pm 0.06$, since we can ignore the uncertainty in K_1. It is worth emphasising that this is an absolute limit, not a 1σ uncertainty.

5.4 The radius of the secondary star

The radius of the secondary is

$$R_2 = \frac{Pv\sin(i)}{2\pi\sin(i)} = 0.40 \pm 0.05 R_\odot/\sin(i). \quad (3)$$

In fact the uncertainty in $\sin(i)$ (4 percent) is smaller than the uncertainty in our measurement of $v_2\sin(i)$, so we take the mid-point of the range in $\sin(i)$ to obtain $R_2 = 0.43 \pm 0.06 R_\odot$.

5.5 The mass and radius of the primary

The analogous formula to equation 1 for the primary is

$$M_1 = \frac{K_2^3 P}{2\pi G \sin^3(i)} \left(1 + \frac{K_1}{K_2}\right)^2, \quad (4)$$

which yields

$$M_1 = \frac{0.91 \pm 0.01 M_\odot}{\sin^3(i)}. \quad (5)$$

The uncertainty here should be treated with some scepticism as it includes just the uncertainty in K_1, not that from K_2, for reasons discussed in Section 4.1.3. Given our range of inclinations, this leads to a range for M_1 of 1.02 to $1.32 M_\odot$.

The radius of the white dwarf can now be determined from the gravitational redshift $(\gamma_1 - \gamma_2)$ as

$$R_1 = \frac{GM_1}{c(\gamma_1 - \gamma_2)}, \quad (6)$$

where c is the velocity of light. Long & Gilliland (1999) measured γ_1 as 172±15km s^{-1}. If we subtract from this our value for γ_2 of 29 km s^{-1} we derive a gravitational redshift for the white dwarf of 143±15km s^{-1}. We use this in Figure 8 to summarise the constraints on M_1.

6 DISCUSSION

6.1 The Secondary Star

The first question to settle is whether the star lies on the main-sequence mass radius relationship. Although small, the uncertainties cover all the mass-radius relationships given in Figure 2 of Smith & Dhillon (1998). This is still true if we tighten the mass constraint to that given by using the tighter limits on the inclination given by Smak (2001).

Where the problem lies with the secondary star is the spectral type. In Figure 9 we plot the spectral type of field M-stars given in Reid et al. (1995) and Hawley et al. (1996) which have masses in Delfosse et al. (2000) against mass. Given its mass, we would expect the secondary in U Gem to be an M2 star. Interestingly that is exactly the conclusion reached by Harrison et al. (2000) on entirely different

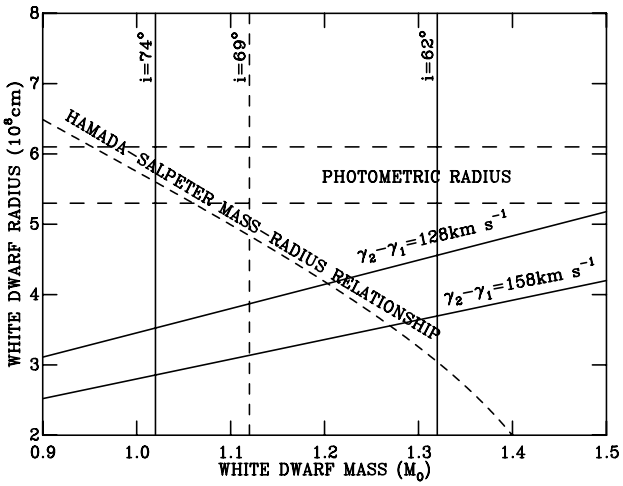

Figure 8. The constraints in the mass-radius plane for the white dwarf. This is essentially an updated version of Figure 7 of Long & Gilliland (1999) and Figure 4 of Long (2000). The gravitational redshift and inclination constrain the white dwarf to lie within the box delineated by the solid lines. The white dwarf mass is primarily limited by the measurement of K_2 and the inclination limits of 62 to 74 degrees. (There is, in addition, a weaker dependence on q.) Our measurement of the gravitational redshift to the white dwarf restricts the white dwarf to lie between the two lines marked $\gamma_2 - \gamma_1$. The Hamada-Salpeter mass-radius relationship intersects the box, but is somewhat above the radius predicted by the inclination of 69 degrees which originates from studies of the bright spot. The photometric radius (see text) lies between the two horizontal dotted lines, well above the dynamical limits.

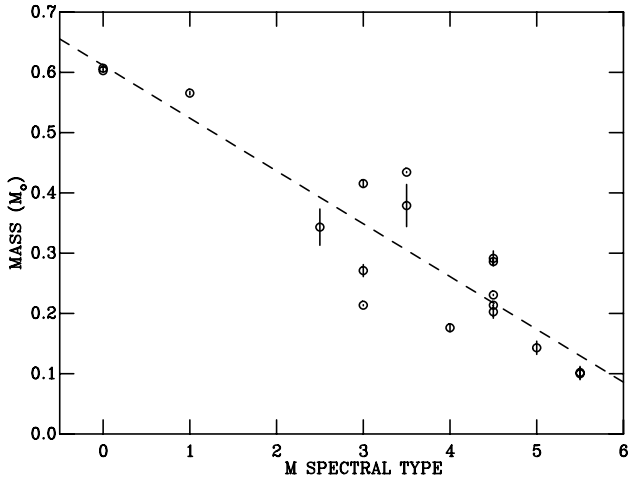

Figure 9. The mass of M-type field stars as a function of spectral type from Reid et al. (1995) and Hawley et al. (1996) The dotted line is an unweighted linear fit.

grounds. They showed that the absolute magnitude of the secondary star, and the optical/IR spectral energy distribution were well matched by an M2 star with a white dwarf and a faint, power-law accretion continuum. The problem arises because our best fits of spectral type standards to the spectrum of U Gem imply a spectral type of M4 or M5 (all our spectral types are also from Reid et al. 1995). This is perfectly consistent with the results obtained by similar methods by other workers; M4$^+$ (Friend et al. 1990) and M4.5 (Wade 1981; Stauffer et al. 1979).

One may be able to solve this inconsistency if the secondary star in U Gem has a high metallicity. Figure 9 shows that there is a spread in spectral type at any given mass. For example, there is an M3.5 star with a mass of 0.415M$_\odot$, which if it were the analogue of the secondary star in U Gem may come close to solving the discrepancy. It is GJ2069A, actually a binary with a mean mass of 0.415M$_\odot$ (Delfosse et al. 1999), and a spectral type of M3.5 (Reid et al. 1995). Delfosse et al. (2000) suggest that the late spectral type is due to high metallicity, with [M/H]=0.5. One could then explain our cross-correlation results as follows. If the star is of high metallicity, the lines will be closer to saturation than one might expect for an M2 star. As such the line shapes and relative depths of the bandheads will be closer to that of a later type, solar metallicity star, which has stronger lines. The χ^2 fitting procedure, which attempts to match line shapes and bandheads (but not the equivalent widths because of the accretion continuum) will give a lower χ^2_ν for the later spectral type star. Further evidence that this is the case comes from the fraction of the light which our fitting procedure gives as originating from the secondary star (see Table 2). The fraction increases with earlier spectral types, already reaching 100 percent for M3, and presumably would be even higher for an M2 spectral type standard. Such behaviour is simply explained if the secondary is an M2 star with line strengths enhanced by a high metallicity.

There is one potential problem with the high metallicity explanation, in that it would also reduce the absolute magnitude. Ribas (2003) does indeed find that the absolute K-band magnitude of GJ2069A is 0.35 mag fainter than stars of comparable mass. However, such a small change in absolute magnitude corresponds to about a third of a spectral sub-class, and so would not affect the conclusions of Harrison et al. (2000), based on the absolute magnitude of U Gem.

In summary, the observations are consistent with the idea that the secondary star in U Gem is an M2 dwarf with high metallicity. In terms of mass, radius and luminosity it is indistinguishable from similar field M dwarfs.

6.2 The broader "cool secondary" problem

There have been suggestions for many years that the secondary stars in CVs may be too cool for their mass. If we extrapolate from the observations of U Gem, then the problem is not that they are too cool, but simply have a spectral type which is later than that for a solar metallicity star of the same effective temperature. Smith & Dhillon (1998) apparently showed that such claims were incorrect, by comparing the mass-spectral-type relation for CV secondary stars with that for field stars, derived from eclipsing binaries. Their argument was that the spread in spectral types of CV secondaries at a given mass was matched by the spread in field stars. For the field M-stars, the spread they referred to was driven by the high mass for the probably-metal-rich GJ2069A. Conversely, the spread in spectral types for the CV secondary stars was driven by the high masses of two objects. First U Gem, whose mass this work revises down-

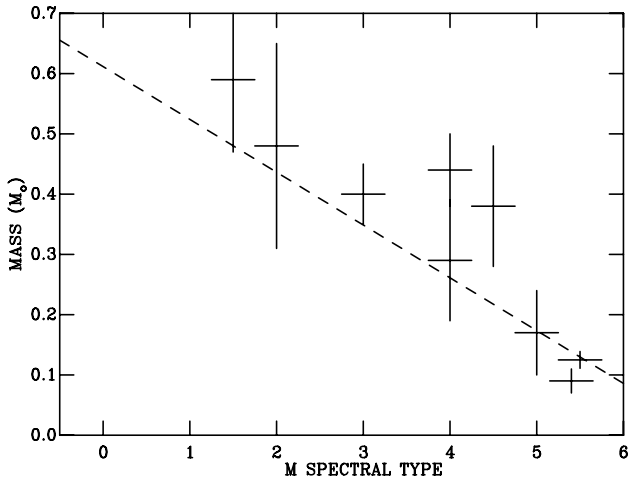

Figure 10. Mass of M-type secondary stars in CVs as a function of spectral type from Smith & Dhillon (1998) with revisions for U Gem from this work and IP Peg from Beekman et al. (2000). The dotted line is an unweighted linear fit to the field star data of Figure 9.

wards by 30 percent, and secondly IP Peg, whose mass we revised downwards by almost a factor two in Beekman et al. (2000). We have plotted therefore, in Figure 10, the spectral types for CVs with well determined secondary star masses from Smith & Dhillon (1998) with the revisions for U Gem and IP Peg.

Compared with the data available to Smith & Dhillon (1998), there are now many more accurate field star masses, which we have represented in Figure 10 by an unweighted linear fit. The data suggest that, on average, CV secondaries show a tendency to be over-massive for their spectral types. For example, two of the best determinations, IP Peg and U Gem lie at later spectral types than any field object of similar mass. However, this tendency is small (up to about 2 sub-types) and we agree with Smith & Dhillon (1998) that it is the spread in both the field and CV mass/spectral-type relation, rather than any systematic shift, which precludes the use of mass to spectral-type conversions.

There is current theoretical interest in explaining differences between the observed spectral type and the spectral type predicted by the mass of the star (e.g. Kolb et al. 2001). Our results suggest strongly that any such comparison should be carried out between the models and the photometric spectral type, not the spectroscopic one.

6.3 The White Dwarf

We can use our data to test whether the white dwarf properties are similar to those of field white dwarfs. From our data we can test whether it follows a similar mass radius relationship, and whether its luminosity is that expected for its radius and temperature.

To begin with the mass and radius, we have placed on Figure 8 the Hamada-Salpeter mass-radius relationship as parameterised in Anderson (1988). The range of masses and radii implied by the gravitational redshift in combination with the estimates of the inclination are consistent with the Hamada-Salpeter mass-radius relationship. To make all three consistent implies that the "preferred" inclination of 69 degrees (see Section 5.2) seems to be a little too high. However, this conclusion should be tempered with the realisation that field white dwarfs do not appear to follow this relationship closely. Provencal et al. (1998) show that a large number of white dwarfs apparently fall below this relationship, for reasons which are not clear. The factor is up to about 20 percent, which would be sufficient to solve the discrepancy.

One can also estimate the radius from the FUV spectrum and the distance, as was discussed by Long & Gilliland (1999) and Long (2000). Their results, scaled to reflect the new (and larger) astrometric distance of 100pc (Harrison et al. 2004) are also plotted in Figure 8, and indicate a white dwarf radius of 5.7×10^8cm, which we shall refer to as the photometric radius. The uncertainties in this value are small. The uncertainty in the parallax is about 5 percent, and hence contributes 5 percent to the uncertainty in radius. The overall flux level of the HST spectra is uncertain at the 10 percent level, which translates to a further 5 percent uncertainty in radius. This yields an overall uncertainty of 7 percent, or a radius of $5.7 \pm 0.4 \times 10^8$cm. This figure is inconsistent with our value of the radius derived from $\gamma_2 - \gamma_1$. This discrepancy is not straightforward to resolve. Lower inclinations give a larger white dwarf radius, so if we take the lowest possible inclination, we still find that $\gamma_2 - \gamma_1$ implies a radius of only $4.13 \pm 0.44 \times 10^8$cm, which differs from the photometric radius at the 2.5σ level. Worse still this would place the white dwarf well above the Hamada-Salpeter radius. If we wish to make the photometric radius consistent with the Hamada-Salpeter radius we require $\gamma_2 - \gamma_1$=80km s^{-1}, which is far outside our error bars.

One possible solution is to posit another UV component in the spectrum (Long et al. 1993). The UV flux in U Gem declines slowly during quiescent intervals. However, as was first noted by Kiplinger et al. (1991), the decline in flux is not consistent with the temperature derived from modelling the spectra in terms of a uniform temperature white dwarf. When modelled as a single temperature white dwarf the temperature of the white dwarf is hottest and the radius smallest just after outburst. Long et al. (1993, 1995) suggested, based on 850-1850Å spectra obtained with the Hopkins Ultraviolet Telescope, that the discrepancy might be resolved if the outburst left behind a hot accretion belt on the surface of the white dwarf that slowly decayed. Other possibilities for the second component include emission caused by heating of the white dwarf due to ongoing accretion and/or emission from the inner disc. The inclusion of a second component does sometimes reduce the estimated radius of the white dwarf. However, it is difficult to make such a second component quantitatively plausible. For example a white dwarf with a temperature of 30,000 K and a radius of 4×10^8 cm at a distance of 100 pc would produce only about half of the observed UV flux. As a result, to reduce the inferred radius from 5.7×10^8 to 4×10^8cm requires either that the second component contributes about the same flux as the first component, or that the second component causes the temperature of the first component to be underestimated by order 10,000K, or some combination thereof. Based on our experience and the fact that the white dwarf in U Gem

is by far the best studied white dwarf in a dwarf nova, we are sceptical the errors in the existing spectral analyses are large enough to easily reconcile the two ways of estimating the radius of the white dwarf in U Gem.

In summary, the mass and radius of the white dwarf deduced from the gravitational redshift and binary inclination are consistent with those for field stars, but inconsistent with the radius deduced from the astrometric parallax, temperature and observed UV flux.

6.4 Determining q using $v_2$sin(i)

A technique frequently used in studies of cataclysmic variables is to measure q using $v_2\sin(i)$ and K_2. This uses the fact that

$$\frac{v_2\sin(i)}{K_2} = (1+q)\frac{R_2}{a}. \quad (7)$$

Since we have a measure of q which is independent of $v_2\sin(i)$ we can test the validity of this method. We find that $v_2\sin(i)/K_2 = 0.38 \pm 0.05$. If we now use the approximation for R_2/a due to Eggleton (1983) we find that $q = 0.41 \pm 0.03$, which is consistent with (though less accurate than) the value determined using K_1, giving us confidence in parameters determined for this and other systems using $v_2\sin(i)$.

7 CONCLUSIONS

Our primary conclusions are as follows.

- The mass and radius of the white dwarf in U Gem determined from the gravitational redshift and inclination are indistinguishable from a field white dwarf. However, the radius deduced from the UV spectrum and astrometric parallax is inconsistent with this kinematic determination. Further analysis and/or observations are required to understand whether the kinematic and spectroscopic information can be reconciled. This is important since U Gem is the prototypical dwarf nova.
- The secondary star in U Gem is indistinguishable in mass and radius from a field M2 dwarf. However, the spectroscopic spectral type is later than might be expected, but this can be explained if it is of higher than solar metallicity.
- The M-stars in cataclysmic variables seem, as a group to be around 1 spectral sub-type cooler than might be expected from their mass or radius. There is a scatter about the mean mass/spectral type relationship of about a sub-type.

On our way to reaching these conclusions we have discovered the following.

- We have tested the determination of the mass ratio using the rotational velocity of the secondary star, and shown (at least in the case of U Gem) it gives answers consistent with other data.
- However, the uncertainty in the derived rotational velocity is dominated by the uncertainty in choosing which spectral type star should used for the cross-correlation.
- The uncertainty in the radial velocity semi-amplitude of the secondary star is dominated by effects at the few km s^{-1} level which are due to the asphericity of the secondary star and non-uniformities in the distribution of the line flux over its surface.

ACKNOWLEDGEMENTS

The Isaac Newton Telescope is operated on the island of La Palma by the Isaac Newton Group in the Spanish Observatorio del Roque de los Muchachos of the Instituto de Astrofisica de Canarias. We thank Stuart Littlefair for useful discussions, and the referee Robert Smith for a careful reading and useful suggestions. Computing was performed on the Exeter node of the Starlink network, funded by PPARC.

REFERENCES

Anderson N., 1988, ApJ, 325, 266
Beekman G., Somers M., Naylor T., Hellier C., 2000, MNRAS, 318, 9
Brett J. M., Smith R. C., 1993, MNRAS, 264, 641
Davey S., Smith R. C., 1992, MNRAS, 257, 476
Delfosse X., Forveille T., Mayor M., Burnet M., Perrier C., 1999, A&A, 341, L63
Delfosse X., Forveille T., Ségransan D., Beuzit J.-L., Udry S., Perrier C., Mayor M., 2000, A&A, 364, 217
Eggleton P. P., 1983, ApJ, 268, 368
Friend M. T., Martin J. S., Smith R. C., Jones D. H. P., 1990, MNRAS, 246, 637
Friend M. T., Smith R. C., Martin J. S., Jones D. H. P., 1988, MNRAS, 233, 451
Gizis J. E., Reid I. N., Hawley S. L., 2002, AJ, 123, 3356
Harrison T. E., Johnson J. J., McArthur B. E., Benedict G. F., Szkody P., Howell S. B., Gelino D. M., 2004, AJ, 127, 460
Harrison T. E., McNamara B. J., Szkody P., Gilliland R. L., 2000, AJ, 120, 2649
Hawley S. L., Gizis J. E., Reid I. N., 1996, AJ, 112, 2799
Horne K., 1986, PASP, 98, 609
Kiplinger A. L., Sion E. M., Szkody P., 1991, ApJ, 366, 569
Kolb U., King A. R., Baraffe I., 2001, MNRAS, 321, 544
Littlefair S. P., Dhillon V. S., Marsh T. R., Harlaftis E. T., 2001, MNRAS, 327, 475
Long K. S., 2000, New Astronomy Review, 44, 125
Long K. S., Blair W. P., Bowers C. W., Davidsen A. F., Kriss G. A., Sion E. M., Hubeny I., 1993, ApJ, 405, 327
Long K. S., Blair W. P., Raymond J. C., 1995, ApJ, 454, L39+
Long K. S., Gilliland R. L., 1999, ApJ, 511, 916
Lucy L. B., 1967, Zeitschrift fur Astrophysics, 65, 89
Marcy G. W., Lindsay V., Wilson K., 1987, PASP, 99, 490
Marsh T. R., Horne K., Schlegel E. M., Honeycutt R. K., Kaitchuck R. H., 1990, ApJ, 364, 637
Paczynski B., 1977, ApJ, 216, 822
Provencal J. L., Shipman H. L., Hog E., Thejll P., 1998, ApJ, 494, 759
Reid I. N., Hawley S. L., Gizis J. E., 1995, AJ, 110, 1838
Ribas I., 2003, A&A, 398, 239
Shahbaz T., 1998, MNRAS, 298, 153
Shahbaz T., Naylor T., Charles P. A., 1993, MNRAS, 265, 655
Smak J. I., 2001, Acta Astronomica, 51, 279
Smith D. A., Dhillon V. S., 1998, MNRAS, 301, 767
Stauffer J., Spinrad H., Thorstensen J., 1979, PASP, 91, 59
Wade R. A., 1981, ApJ, 246, 215
Warner B., Nather R. E., 1971, MNRAS, 152, 219

Webb N. A., Naylor T., Ioannou Z., Charles P. A., Shahbaz T., 2000, MNRAS, 317, 528
Webb N. A., Naylor T., Jeffries R. D., 2002, ApJ, 568, L45

This paper has been typeset from a TEX/ LATEX file prepared by the author.